Mathematical Engineering

Andreas Rauh
Luise Senkel *Editors*

Variable-Structure Approaches

Analysis, Simulation, Robust Control and Estimation of Uncertain Dynamic Processes

Springer

Mathematical Engineering

More information about this series at http://www.springer.com/series/8445

Andreas Rauh · Luise Senkel
Editors

Variable-Structure Approaches

Analysis, Simulation, Robust Control and Estimation of Uncertain Dynamic Processes

Springer

Editors
Andreas Rauh
Universität Rostock
Rostock, Mecklenburg-Vorpommern
Germany

Luise Senkel
Universität Rostock
Rostock, Mecklenburg-Vorpommern
Germany

ISSN 2192-4732 ISSN 2192-4740 (electronic)
Mathematical Engineering
ISBN 978-3-319-31537-9 ISBN 978-3-319-31539-3 (eBook)
DOI 10.1007/978-3-319-31539-3

Library of Congress Control Number: 2016936579

Printed on acid-free paper

This Springer imprint is published by Springer Nature
The registered company is Springer International Publishing AG Switzerland

Preface

In recent years, numerous variable-structure approaches have been developed for the control of nonlinear dynamic systems and for the model-based estimation of non-measurable states and parameters. These approaches typically make use of first-order as well as higher order sliding mode techniques and related procedures that are characterized by a variable-structure nature. One of their main advantages is the inherent proof of asymptotic stability. This stability proof is either performed offline during the corresponding controller and estimator design or online by the real-time evaluation of a suitable candidate for a Lyapunov function.

The methodological framework for variable-structure control and estimation approaches is quite well developed in the case of continuous-time and discrete-time systems, for which process models are accurately known.

Nevertheless, research efforts are still necessary to make the corresponding procedures applicable when only worst-case bounds are available for specific parameters. This type of uncertainty is often caused by non-negligible, however, inevitable manufacturing tolerances. Moreover, significant stochastic disturbances—for example, as a result of measurement noise—may act as further system inputs in many practically relevant applications. To enhance robustness in such cases, it is possible to combine variable-structure approaches with techniques which are for instance based on interval analysis, stochastic differential equations, or linear matrix inequalities.

This book aims at presenting current research activities in the field of robust variable-structure systems. The scope equally consists in highlighting novel methodological aspects as well as in presenting the use of variable-structure techniques in industrial applications including their implementation on hardware for real-time control.

Besides variable-structure approaches for the design of feedback control strategies and state estimation procedures, computational techniques for simulation—as included in predictive controllers—robustness and stability analysis, as well as for the identification of system models which are characterized by an inherent variable-structure behavior are included. Such models may result from a mathematical representation of state-dependent transitions between various state-space

representations, for example, due to faults of selected system components or due to different system models depending on the current operating conditions of the considered system.

Rostock
January 2016

Andreas Rauh
Luise Senkel

Acknowledgments

The editors of this special volume on *Variable-Structure Approaches for Analysis, Simulation, Robust Control and Estimation of Uncertain Dynamic Processes* would like to thank all authors for their high-quality contributions. Moreover, we would like to thank all researchers who supported us by reviewing the individual book chapters and by providing invaluable comments and suggestions for improvements. Finally, we would like to thank Prof. Dr. Claus Hillermeier (University of the Federal Armed Forces, Munich, Germany) and Dr. Jan-Philip Schmidt (Springer–Verlag) for supporting our idea to publish this collection of current research articles in the book series *Mathematical Engineering*.

Contents

Part I
Sliding Mode Control for Continuous and Discrete-Time Systems

In the first part of this book, scientific works are presented which focus on solving control tasks for nonlinear and uncertain dynamic systems by the application as well as the novel development of sliding mode control techniques. In Chap. 1, Saif Siddique Butt, Hao Sun, and Harald Aschemann describe a comparison of backstepping-based sliding mode techniques and adaptive backstepping approaches for the design of robust controllers of a twin rotor helicopter. In contrast to the continuous-time design in the first chapter, Chap. 2 authored by Piotr Leśniewski and Andrzej Bartoszewicz deals with the robust, discrete-time congestion controller design for a single virtual circuit in connection-oriented communication networks. Andreas Rauh and Luise Senkel develop and implement novel interval methods for the robust sliding mode control synthesis of high-temperature fuel cells. Besides the influence of uncertain but bounded parameters and disturbances, the handling of state and input constraints is explicitly addressed in this Chap. 3. Further methodological extensions of interval-based sliding mode controllers are presented in Chap. 4 by Luise Senkel, Andreas Rauh, and Harald Aschemann. It deals with the experimental and numerical validation of a reliable sliding mode control strategy considering uncertainty with the help of interval arithmetic in a real-time capable implementation.

Comparison of Backstepping-Based Sliding Mode and Adaptive Backstepping for a Robust Control of a Twin Rotor Helicopter

Saif Siddique Butt, Hao Sun and Harald Aschemann

Abstract In this contribution, two robust MIMO backstepping control approaches for a twin rotor aerodynamic system (TRAS) test-rig are considered. The TRAS represents a nonlinear system with significant couplings. A nonlinear multibody model of the TRAS with lumped unknown disturbance torques is derived using Lagrange's equations. Herewith, both a backstepping-based sliding mode control and an adaptive backstepping control are designed to track desired trajectories for the azimuth angle and the pitch angle. An explicit expression is derived for the reaching time in the case of the backstepping-based sliding mode control. In order to estimate immeasurable angular velocities and unknown disturbance torques for the backstepping-based sliding mode control, a discrete-time extended Kalman filter (EKF) is employed. For the adaptive backstepping, a robust sliding mode differentiator is used instead to estimate the angular velocities. Moreover, in the adaptive backstepping control approach, the disturbance compensation is realised with the help of additional adaptive control parts driven by the tracking errors of the controlled variables. The overall stability of the proposed controllers in combination with the corresponding estimator is investigated thoroughly by simulations. Furthermore, in order to validate the proposed control schemes, experiments are performed on the dedicated test-rig and a comparison of the two proposed control structures is provided as well.

S.S. Butt · H. Sun (✉) · H. Aschemann
Chair of Mechatronics, University of Rostock, Justus-von-Liebig-Weg 6, 18059 Rostock, Germany
e-mail: hao.sun@uni-rostock.de

S.S. Butt
e-mail: saif.butt@uni-rostock.de

H. Aschemann
e-mail: harald.aschemann@uni-rostock.de

A. Rauh and L. Senkel (eds.), *Variable-Structure Approaches*,
Mathematical Engineering, DOI 10.1007/978-3-319-31539-3_1

1 Introduction

A twin rotor aerodynamic system (TRAS) with two degrees of freedom (DOF) developed by INTECO [10], Poland, is depicted in Fig. 1. It consists of a beam with two propellers—the main and the tail propellers—at both ends of the beam, driven by DC motors. The beam is pivoted in a cardanic joint and can rotate within confined regions in the horizontal and vertical planes. These limitations arise due to the mechanical construction of the test-rig. Two levers with counter-weights at their ends are fixed to the beam at the pivot. The counter-weights determine the steady-state pitch angle without propeller actuation. Two velocity sensors are coupled with the PWM-driven DC motors for the main and tail rotors. Moreover, two incremental encoders are directly mounted at the pivot point of the beam in order to measure the relative angle of the beam. Based on the mechanical construction, the TRAS test-rig possesses 2-DOF. The first DOF characterises the horizontal rotation of the frame using the azimuth angle, whereas the second one is given by the pitch angle describing the inclination of the frame. In a real helicopter the aerodynamic force is adjusted by changing the angle of attack. The TRAS, however, uses a changing angular velocity for this purpose.

The 2-DOF helicopter system imposes challenging control problems due to its given nonlinearities and significant couplings between both degrees of freedom. To remedy such drawbacks and achieve satisfactory control performance for the accurate tracking of desired trajectories for the azimuth and pitch angles, a control-oriented model of the system is useful. In the past decade, several contributions related to the modelling and experimental identification of similar 2-DOF helicopter set-ups have been published [1, 2, 7, 18, 19]. The methods proposed therein correspond to typical set-ups provided by different manufacturers, various model-based and

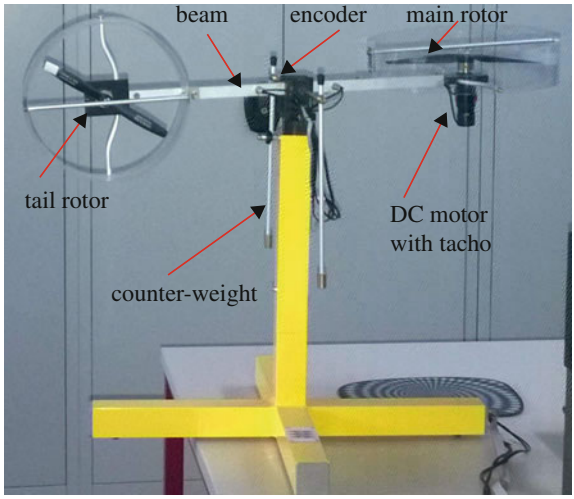

Fig. 1 TRAS test-rig at the Chair of Mechatronics

artificial-intelligence-based methods, e.g. radial basis function, neural networks and genetic algorithms. In [18], a complete mathematical description of the TRAS based on the both the Newton–Euler approach and Lagrange's equations is presented. However, the mechanical construction of the test set-up therein differs from the TRAS test-rig used in this contribution. A complete mathematical description of the TRAS set-up is derived in the form of a detailed ninth-order model in the work of [8]. Regarding the control of the TRAS, the authors performed a simulation study using a nonlinear predictive control for the ninth-order system model. In [16], a feedback linearising control scheme is presented for the pitch motion only. Therein, the yaw position is not considered as a DOF. Lopez et al. [15, 17] proposed an H_∞-controller for the helicopter dynamics. In [4], a nonlinear control-oriented model of the TRAS manufactured by INTECO along with a multi-variable flatness-based control scheme has been proposed for TRAS. However, the influence of the mass moments of inertia of the rotating beam on the kinetic energy of the system has not been addressed. For the estimation of disturbance torques and unmeasured states, the authors employed a discrete-time EKF. In [3, 5], a sliding mode and an integral sliding mode control are considered, respectively, allowing to deal with couplings inherent in the twin rotor dynamics. Following the idea of a cascaded control structure, it is suitable to employ backstepping techniques for the control design. Both the design and the implementation of the separate controllers are simplified in comparison to a central control structure. Disturbances are taken into account by an adaptive backstepping control approach. Although an adaptive control scheme based on backstepping control is already proposed in [11], the authors focus especially on the derivation of adaptive control laws for a set of uncertain parameters within the pitch and the azimuth dynamics. The adaptive backstepping control design guarantees global stabilisation. Nevertheless, due to the large number of adaptive laws, the convergence of the parameter estimates to their true values cannot be guaranteed. This may lead to unrealistic values of the parameters [20]. One possible way to handle this situation is to introduce a lumped disturbance term that represents the overall parameter uncertainty and to design a parameter update law for this lumped disturbance. Therefore, in the given contribution, the parameter uncertainty and the model uncertainty are combined together as a lumped disturbance torque for each axis. As a result, the adaptive laws are needed only for these lumped disturbance torques rather than for the individual parameter uncertainty.

As mentioned earlier, the TRAS system is affected by parameter uncertainty due to the limited knowledge of the true parameter values and unknown disturbances. Hence, a robust way of controlling such a system is the application of variable structure control techniques [23]. For this purpose, a backstepping-based sliding mode control scheme is proposed and investigated as well. Although many significant contributions are already available for the control design of the TRAS, a lot of questions are worth further investigations. This in particular includes the analysis of a damping term in the sliding mode control law concerning the reaching time. One of the main contributions regarding the backstepping-based sliding mode control is the derivation of the corresponding reaching time which—according to the best of the authors knowledge—has not been addressed in previous works.

This chapter is structured as follows: in Sect. 2, the mathematical description of the nonlinear control-oriented model of the TRAS based on Lagrange's equations is presented. Based on the derived system model, two alternative control strategies are described in Sect. 3: a backstepping-based sliding mode control and an adaptive backstepping control. For each control strategy, the asymptotic stability is shown by Lyapunov techniques. Moreover, the overall closed-loop error dynamics for each control scheme emphasise the asymptotic stability. In Sect. 4, a discrete-time EKF is designed to estimate the angular velocities as well as the unknown lumped disturbance torques, which are required for the backstepping-based sliding mode control structure. For the adaptive backstepping control structure, a robust sliding mode differentiator is proposed that provides estimates for the angular velocities. The implementation of the proposed two control strategies together with their corresponding estimators are explained as well in this section. In Sect. 5, relevant simulation results and experimental investigations from the TRAS test-rig are presented and discussed. Finally, conclusions and outlook are provided in Sect. 6.

2 Control-Oriented Model of TRAS

Dynamic system modelling plays a key role in modern control engineering. For a model-based control design, an accurate mathematical description of the system dynamics is essential to improve the overall system performance. For the control-oriented modelling of the TRAS an inertial reference frame is defined and the dynamic model is derived using Lagrange's equations.

The multibody system model for the TRAS consists of a beam, point masses for the two rotors and point masses for the two counterbalances. The mathematical analysis starts with assigning a right-hand coordinate system with the origin O placed at the pivot point of the beam as depicted in Fig. 2. The pitch angle is denoted by ψ and the azimuth angle is given by ϕ. The distance of the main rotor from the origin O is characterised by the length l_m, whereas the distance of the tail rotor from the origin O is given by l_t. The lumped masses corresponding to the main rotor and the tail rotor are denoted by m_m and m_t, respectively. Moreover, l_{cw} represents the relevant length of the two levers with a lumped mass m_{cw} as counter-weight at their end. The propulsive forces acting on the main rotor and the tail rotor are denoted by F_ψ and F_ϕ, respectively. The corresponding position vectors $\mathbf{r}_m$ for the main rotor and $\mathbf{r}_t$ for the tail rotor are given by

$$\mathbf{r}_m = \begin{bmatrix} l_m \cos\psi \cos\phi \\ l_m \cos\psi \sin\phi \\ l_m \sin\psi \end{bmatrix}, \quad \mathbf{r}_t = \begin{bmatrix} -l_t \cos\psi \cos\phi \\ -l_t \cos\psi \sin\phi \\ -l_t \sin\psi \end{bmatrix}. \tag{1}$$

Likewise, the position vectors $\mathbf{r}_{cw1}$ and $\mathbf{r}_{cw2}$ for the counter-weights result in

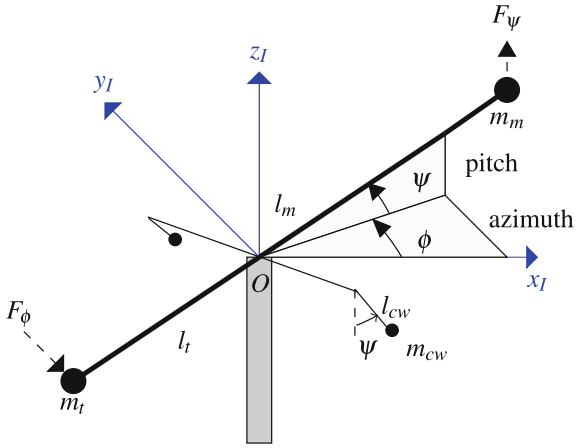

Fig. 2 Free body diagram of TRAS

$$\mathbf{r}_{cw1} = \begin{bmatrix} -l_{cw}\sin\psi\sin\phi \\ -l_{cw}\sin\psi\cos\phi \\ -l_{cw}\cos\psi \end{bmatrix}, \ \mathbf{r}_{cw2} = \begin{bmatrix} l_{cw}\sin\psi\sin\phi \\ l_{cw}\sin\psi\cos\phi \\ -l_{cw}\cos\psi \end{bmatrix}. \tag{2}$$

The overall kinetic energy T of TRAS is determined with the help of velocity vectors as well as the mass moments of inertia of the rotating beam. The kinetic energy of the TRAS in terms of the generalised coordinates is expressed as

$$\begin{aligned} T &= \frac{m_m}{2}\dot{\mathbf{r}}_m^2 + \frac{m_t}{2}\dot{\mathbf{r}}_t^2 + \frac{m_{cw}}{2}(\dot{\mathbf{r}}_{cw1}^2 + \dot{\mathbf{r}}_{cw2}^2) + \frac{1}{2}J_z\dot{\phi}^2 + \frac{1}{2}J_x\dot{\psi}^2 \\ &= \frac{1}{2}\Big((m_m l_m^2 + m_t l_t^2)(\dot{\phi}^2\cos^2\psi + \dot{\psi}^2) + m_{cw}l_{cw}^2(\dot{\phi}^2\sin^2\psi + \dot{\psi}^2) + J_z\dot{\phi}^2 + J_x\dot{\psi}^2\Big), \end{aligned} \tag{3}$$

where the square of the velocity components along the corresponding axes are calculated using the standard vector dot product identity, i.e. $\dot{\mathbf{r}}^2 = \dot{\mathbf{r}}^T \cdot \dot{\mathbf{r}}$. The parameters J_x and J_z denote the moment of inertias of the rotating beam w.r.t. the body-fixed x-axis and z-axis, respectively. Similarly, the overall potential energy U of the point mass system is given as

$$U = g\Big((m_m l_m - m_t l_t)\sin(\psi) + 2m_{cw}l_{cw}(1-\cos(\psi))\Big) + \frac{1}{2}k_\phi\,\phi^2. \tag{4}$$

Here, g is the gravitational constant. The parameter k_ϕ is used to model the restoring energy due to the elasticity in the cable. The Lagrangian of the system is defined as the difference between the kinetic energy and the potential energy, i.e.

$$L = T - U.$$

Finally, Lagrange's equations including non-conservative forces result in [9]

$$\frac{d}{dt}\left(\frac{\partial L}{\partial \dot{q}}\right) - \frac{\partial L}{\partial q} = \tau_q - \frac{\partial R}{\partial \dot{q}}, \quad q = \{\phi, \psi\}, \tag{5}$$

where τ_ϕ and τ_ψ are torques along the azimuth and the pitch axes, respectively. The Rayleigh dissipation function R is given by [9]

$$R = \frac{1}{2}\, c_\phi\, \dot{\phi}^2 + \frac{1}{2}\, c_\psi\, \dot{\psi}^2. \tag{6}$$

Substituting (3), (4) and (6) into (5), the equations of motion for the system become

$$J_\phi \ddot{\phi} = \tau_\phi + J\dot{\phi}\dot{\psi}\sin(2\psi) - k_\phi \phi - c_\phi \dot{\phi}, \tag{7}$$

$$J_\psi \ddot{\psi} = \tau_\psi - g\Big[(m_m l_m - m_t l_t)\cos\psi + 2m_{cw} l_{cw}\sin\psi\Big] - J\frac{\dot{\phi}^2}{2}\sin(2\psi) - c_\psi \dot{\psi}, \tag{8}$$

with the following definition of the mass moments of inertia

$$J_\phi = J_\phi(\psi) = (m_m l_m^2 + m_t l_t^2)\cos^2\psi + 2m_{cw} l_{cw}^2 \sin^2\psi + J_z, \tag{9}$$

$$J_\psi = m_m l_m^2 + m_t l_t^2 + 2m_{cw} l_{cw}^2 + J_x, \tag{10}$$

$$J = m_m l_m^2 + m_t l_t^2 - 2m_{cw} l_{cw}^2. \tag{11}$$

The dynamics of the beam w.r.t. the pitch angle and azimuth angle is strongly nonlinear and contains couplings. The torques τ_ϕ and τ_ψ are combined in the input vector $\mathbf{u} = [\tau_\phi \;\; \tau_\psi]^T$, with

$$\tau_\phi = F_\phi l_t \cos\psi \quad \text{and} \quad \tau_\psi = F_\psi l_m. \tag{12}$$

Here, F_ψ and F_ϕ denote the propulsive forces provided by the main rotor and the tail rotor, respectively. To handle the parameter uncertainty and unknown disturbances, the model is extended with two lumped disturbance torques $\mathbf{z} = [z_\phi \;\; z_\psi]^T$ acting on the azimuth and pitch axes, respectively. With the state vector $\mathbf{x} = [\phi \;\; \dot{\phi} \;\; \psi \;\; \dot{\psi}]^T$, the extended nonlinear state-space model $\dot{\mathbf{x}} = \mathbf{f}(\mathbf{x}, \mathbf{u}, \mathbf{z})$ becomes

$$\begin{bmatrix} \phi \\ \dot{\phi} \\ \psi \\ \dot{\psi} \end{bmatrix} = \begin{bmatrix} \dot{\phi} \\ \frac{1}{J_\phi}\Big(-c_\phi\dot{\phi} - k_\phi\phi + J\dot{\phi}\dot{\psi}\sin(2\psi)\Big) + \frac{l_t\cos(\psi)}{J_\phi}F_\phi + \frac{1}{J_\phi}z_\phi \\ \dot{\psi} \\ \frac{1}{J_\psi}\Big(-c_\psi\dot{\psi} - J\frac{\dot{\phi}^2}{2}\sin(2\psi) - g\big((m_m l_m - m_t l_t)\cos\psi \\ \qquad + 2m_{cw} l_{cw}\sin\psi\big)\Big) + \frac{l_m}{J_\psi}F_\psi + \frac{1}{J_\psi}z_\psi \end{bmatrix}. \tag{13}$$

These disturbance torques, on the one hand, account for parameter uncertainty. On the other hand, the unmodelled effects due to the supply cables and gyroscopic torques as well as the couplings caused by the tail rotor and the main rotor in the case of angular accelerations of the propellers are encompassed by the lumped disturbance torques.

For trajectory tracking, the azimuth angle and the pitch angle are chosen as controlled outputs. The measurement vector $\mathbf{y}_m$ is given by

$$\mathbf{y}_m(t) = \begin{bmatrix} \phi & \psi \end{bmatrix}^T . \tag{14}$$

The nonlinear control-oriented model given in (13) represents a control-affine system. The system under consideration has matched uncertainties, since the unknown disturbance torques appear in the span of the control input. The systematic procedure of backstepping control design, however, allows to achieve global stabilisation under the influence of both matched and mismatched uncertainties. Therefore, in order to track desired trajectories robustly for the azimuth angle as well as the pitch angle, backstepping-based sliding mode control and adaptive backstepping approaches are proposed and investigated thoroughly.

3 Tracking Control Design for the TRAS

The aim of a robust control approach is to accurately track desired trajectories for both the azimuth angle and the pitch angle despite the parameter uncertainty and unknown disturbances. For this purpose, a comparison between two alternative robust nonlinear control strategies based on backstepping techniques—a backstepping-based sliding mode control and an adaptive backstepping control—is carried out. Generally, the backstepping control design is based on a recursive procedure by systematically choosing appropriate control Lyapunov functions, and the corresponding stabilising functions [12]. In the case of backstepping-based sliding mode control, the lumped disturbance torques along with the immeasurable angular velocities are estimated with the help of an EKF. The adaptive backstepping control design, however, includes a dynamic part that involves the derivation of nonlinear adaptive control laws for the estimation of unknown lumped disturbance torques. Thereby, both the robust performance and the trajectory tracking accuracy are improved. For the state estimation within the adaptive backstepping control strategy, robust sliding mode differentiators are employed for the estimation of the angular velocities. The asymptotic stability of the closed-loop systems for both feedback control approaches is proved using Lyapunov methods. Moreover, the stability of the overall control structures—involving the corresponding estimators—is investigated thoroughly by simulations and experiments. The detailed design procedures for both control techniques are presented in the following subsections.

3.1 Backstepping-Based Sliding Mode Control

A backstepping control design is generally carried out in a recursive fashion. The backstepping-based sliding mode control law can be derived in the two following steps:

Step 1:
Given the continuously differentiable reference signals of class C^2 for the azimuth angle ϕ_d and the pitch angle ψ_d, the tracking errors e_ϕ and e_ψ corresponding to the azimuth angle and the pitch angle, respectively, are defined as

$$e_\phi = \phi - \phi_d \text{ and } e_\psi = \psi - \psi_d. \tag{15}$$

Introducing a so-called virtual control input $\boldsymbol{\alpha} = [\alpha_\phi \quad \alpha_\psi]^T$, which has to be chosen properly, the time derivatives of the error dynamics are given by

$$\begin{aligned} \dot{e}_\phi &= \dot{\phi} - \dot{\phi}_d = \alpha_\phi + r_\phi - \dot{\phi}_d, \\ \dot{e}_\psi &= \dot{\psi} - \dot{\psi}_d = \alpha_\psi + r_\psi - \dot{\psi}_d, \end{aligned} \tag{16}$$

with

$$r_\phi = \dot{\phi} - \alpha_\phi \text{ and } r_\psi = \dot{\psi} - \alpha_\psi. \tag{17}$$

The stabilising functions α_ϕ and α_ψ are chosen as

$$\alpha_\phi = -k_\phi e_\phi + \dot{\phi}_d, \quad \alpha_\psi = -k_\psi e_\psi + \dot{\psi}_d, \tag{18}$$

with the strictly positive coefficients k_ϕ and k_ψ. This leads to the error dynamics

$$\dot{e}_\phi = -k_\phi e_\phi + r_\phi, \text{ and } \dot{e}_\psi = -k_\psi e_\psi + r_\psi. \tag{19}$$

Consider a quadratic control Lyapunov function V_1 and its corresponding time derivative,

$$\begin{aligned} V_1 &= \frac{1}{2}e_\phi^2 + \frac{1}{2}e_\psi^2, \\ \dot{V}_1 &= e_\phi \dot{e}_\phi + e_\psi \dot{e}_\psi = -k_\phi e_\phi^2 + e_\phi r_\phi - k_\psi e_\psi^2 + e_\psi r_\psi, \end{aligned} \tag{20}$$

where $e_\phi r_\phi$ and $e_\psi r_\psi$ will be eliminated in the next step. After elimination, the time derivative of the Lyapunov function is negative definite, i.e.

$$\dot{V}_1 = -k_\phi e_\phi^2 - k_\psi e_\psi^2 < 0, \tag{21}$$

hence, the asymptotic stability can be easily established.

Step 2:
Now, the error dynamics r_ϕ and r_ψ are given by

$$\dot{r}_\phi = \ddot{\phi} - \dot{\alpha}_\phi, \quad \text{and} \quad \dot{r}_\psi = \ddot{\psi} - \dot{\alpha}_\psi. \tag{22}$$

From (18) and (19), the following relationships can be obtained, i.e.

$$\dot{\alpha}_\phi = k_\phi^2 e_\phi - k_\phi r_\phi + \ddot{\phi}_d, \quad \text{and} \quad \dot{\alpha}_\psi = k_\psi^2 e_\psi - k_\psi r_\psi + \ddot{\psi}_d, \tag{23}$$

resulting in

$$\begin{aligned} \dot{r}_\phi &= f_2(\mathbf{x}) + \frac{l_t \cos(\psi)}{J_\phi} F_\phi + \frac{1}{J_\phi} z_\phi - k_\phi^2 e_\phi + k_\phi r_\phi - \ddot{\phi}_d, \\ \dot{r}_\psi &= f_4(\mathbf{x}) + \frac{l_m}{J_\psi} F_\psi + \frac{1}{J_\psi} z_\psi - k_\psi^2 e_\psi + k_\psi r_\psi - \ddot{\psi}_d, \end{aligned} \tag{24}$$

where the functions $f_2(\mathbf{x})$ and $f_4(\mathbf{x})$ are defined using the nonlinear control-oriented model (13). They are given by

$$\begin{aligned} f_2(\mathbf{x}) &= \frac{1}{J_\phi}\left(-c_\phi \dot{\phi} - k_\phi \phi + J \dot{\phi}\dot{\psi} \sin(2\psi)\right), \\ f_4(\mathbf{x}) &= \frac{1}{J_\psi}\left(-c_\psi \dot{\psi} - J \frac{\dot{\phi}^2}{2} \sin(2\psi) - g\big((m_m l_m - m_t l_t)\cos\psi + 2 m_{cw} l_{cw} \sin\psi\big)\right). \end{aligned} \tag{25}$$

For the backstepping-based sliding mode control, sliding manifolds need to be defined. Mathematically, the sliding manifolds are expressed as

$$s_\phi(\mathbf{x}) = c_\phi e_\phi + r_\phi\,, \; s_\psi(\mathbf{x}) = c_\psi e_\psi + r_\psi\,. \tag{26}$$

Here, strictly positive coefficients $c_i > 0,\ i \in \{\phi, \psi\}$, are employed. The sliding manifolds $s_\phi(\mathbf{x})$ and $s_\psi(\mathbf{x})$ correspond to the azimuth axis and the pitch axis, respectively. The time derivatives of the sliding manifolds are given by

$$\dot{s}_\phi(\mathbf{x}) = c_\phi \dot{e}_\phi + \dot{r}_\phi\,, \; \dot{s}_\psi(\mathbf{x}) = c_\psi \dot{e}_\psi + \dot{r}_\psi\,. \tag{27}$$

To ensure that the manifolds are reached in a finite period of time and that they are independent of the initial conditions of the system, sufficient reaching conditions

$$s_i(\mathbf{x})\dot{s}_i(\mathbf{x}) < 0, \forall s(\mathbf{x}) \neq 0\,,\ i \in \{\phi, \psi\}\,, \tag{28}$$

have to be fulfilled. A necessary condition for the existence of a sliding mode implies that, $\forall t \geq t_r$ the output trajectory should remain on the sliding surface, i.e., $s_i(\mathbf{x}) =$

$\dot{s}_i(\mathbf{x}) = 0$. Here, t_r denotes the finite reaching time. Hence, to achieve finite-time convergence, the time derivatives of the Lyapunov functions $1/2 \cdot s_i^2(\mathbf{x})$, $i \in \{\phi, \psi\}$, have to fulfil the following reaching conditions

$$s_i(\mathbf{x})\dot{s}_i(\mathbf{x}) \leq s_i(\mathbf{x})(-h_i s_i(\mathbf{x}) - \eta_i \operatorname{sgn}(s_i(\mathbf{x}))) < 0,\ h_i > 0 \text{ and } \eta_i > 0\ ,\ i \in \{\phi, \psi\}\ . \tag{29}$$

The parameters η_i determine the switching height and guarantee that the time-derivative of the Lyapunov functions become negative definite. The introduction of the additional damping terms $-h_i\ s_i(\mathbf{x})$ together with the switching terms ensure a shorter reaching time in comparison to the case where only the switching functions are employed. A detailed mathematical derivation for the reaching condition discussed at the end of this subsection highlights the effectiveness of the damping term.

Define a Lyapunov function V_2 along with its corresponding time differentiation as

$$\begin{aligned} V_2 &= \frac{1}{2}e_\phi^2 + \frac{1}{2}s_\phi^2 + \frac{1}{2}e_\psi^2 + \frac{1}{2}s_\psi^2, \\ \dot{V}_2(\mathbf{x}) &= \underbrace{e_\phi \dot{e}_\phi + s_\phi \dot{s}_\phi}_{\dot{V}_\phi} + \underbrace{e_\psi \dot{e}_\psi + s_\psi \dot{s}_\psi}_{\dot{V}_\psi}. \end{aligned} \tag{30}$$

In order to make the analysis simple, the time derivative of the control Lyapunov function $V_2(\mathbf{x})$ is split into two parts, $\dot{V}_\phi$ and $\dot{V}_\psi$. Considering

$$\dot{V}_\phi = e_\phi \dot{e}_\phi + s_\phi \dot{s}_\phi, \tag{31}$$

$$= e_\phi(-k_\phi e_\phi + r_\phi) + s_\phi\Big(c_\phi(-k_\phi e_\phi + r_\phi) + \dot{r}_\phi\Big), \tag{32}$$

$$= e_\phi(-k_\phi e_\phi + s_\phi - c_\phi e_\phi) + s_\phi\Big(c_\phi(-k_\phi e_\phi + r_\phi) + \dot{r}_\phi\Big), \tag{33}$$

$$\begin{aligned} = -(k_\phi + c_\phi)e_\phi^2 + s_\phi\Big(e_\phi + c_\phi(-k_\phi e_\phi + r_\phi) + f_2(\mathbf{x}) + \frac{l_t \cos(\psi)}{J_\phi}F_\phi \\ + \frac{1}{J_\phi}z_\phi - k_\phi^2 e_\phi + k_\phi r_\phi - \ddot{\phi}_d\Big). \end{aligned} \tag{34}$$

With the following choice of the control input F_ϕ, i.e.

$$\begin{aligned} F_\phi = \Big(-h_\phi s_\phi - \eta_\phi \operatorname{sgn}(s_\phi) - e_\phi - c_\phi(-k_\phi e_\phi + r_\phi) - f_2(\mathbf{x}) - \frac{1}{J_\phi}z_\phi \\ + k_\phi^2 e_\phi - k_\phi r_\phi + \ddot{\phi}_d\Big)\frac{J_\phi}{l_t \cos(\psi)}\ , \end{aligned} \tag{35}$$

the time derivative of the Lyapunov function is negative definite

$$\dot{V}_\phi = -(k_\phi + c_\phi)e_\phi^2 - h_\phi s_\phi^2 - \eta_\phi s_\phi \,\mathrm{sgn}(s_\phi) < 0. \tag{36}$$

It is worth mentioning that the singularity condition due to $\psi = \pm\pi/2$ does not arise in the real set-up which is fortunately outside the range of feasible pitch angles because of the mechanical design of the test-rig.

Likewise, the control input F_ψ for the main rotor can be determined based on the design procedure already described in detail for the control input F_ϕ. Therefore, the following expression is obtained for the F_ψ, i.e.

$$F_\psi = \Bigg(-h_\psi s_\psi - \eta_\psi \,\mathrm{sgn}(s_\psi) - e_\psi - c_\psi(-k_\psi e_\psi + r_\psi) - f_4(\mathbf{x}) - \frac{1}{J_\psi} z_\psi + k_\psi^2 e_\psi - k_\psi r_\psi + \ddot{\psi}_d\Bigg)\frac{J_\psi}{l_m}. \tag{37}$$

With this choice of the control input, the time derivative of the Lyapunov function V_ψ is

$$\dot{V}_\psi = -(k_\psi + c_\psi)e_\psi^2 - h_\psi s_\psi^2 - \eta_\psi s_\psi \,\mathrm{sgn}(s_\psi) < 0. \tag{38}$$

Hence, the time derivative of the control Lyapunov function from (30) can be rewritten as

$$\dot{V}_2(\mathbf{x}) = -(k_\phi + c_\phi)e_\phi^2 - h_\phi s_\phi^2 - \eta_\phi |s_\phi| - (k_\psi + c_\psi)e_\psi^2 - h_\psi s_\psi^2 - \eta_\psi |s_\psi| < 0. \tag{39}$$

Since all the coefficients are positive, the time derivative of the Lyapunov function remains negative definite. As a consequence, the asymptotic stability of the system is guaranteed.

In order to proof a convergence in finite time to the sliding manifold, i.e. $s(\mathbf{x}) = \dot{s}(\mathbf{x}) = 0$, a detailed mathematical analysis is provided in the following.

Proof of Finite Reaching Time

For brevity, only the sliding manifold regarding the azimuth angle is considered. According to Lyapunov's stability theory, the existence as well as the reaching conditions for a sliding mode can be summarised as follows: if there exists a Lyapunov function $V_{s,\phi}$ with a negative-definite time-derivative [12, 20], i.e.

$$V_{s,\phi} = \frac{1}{2} s_\phi^2, \tag{40}$$

$$\dot{V}_{s,\phi} = s_\phi \dot{s}_\phi < 0 \quad \text{for } s_\phi \neq 0, \tag{41}$$

asymptotic stability can be ensured. To achieve finite-time convergence, however, the time derivative of the Lyapunov function has to fulfil the following reaching

condition

$$\dot{V}_{s,\phi} = s_\phi \dot{s}_\phi \leq s_\phi \left(-h_\phi s_\phi - \eta_\phi \operatorname{sgn}(s_\phi) \right) < 0. \tag{42}$$

The parameter $\eta_\phi > 0$ determines the switching height and guarantees that the time derivative of the Lyapunov function becomes negative definite. Moreover, the introduction of the damping constant $h_\phi > 0$ leads to fast finite-time convergence to the sliding manifold as shown in the sequel. To determine the reaching time t_r, inequality (42) can be rewritten in terms of $V_{s,\phi}$ as

$$\dot{V}_{s,\phi} + 2h_\phi V_{s,\phi} \leq -\sqrt{2}\eta_\phi \sqrt{V_{s,\phi}}. \tag{43}$$

This inequality is in the form of a generalised Bernoulli's differential equation and can be easily transformed to a first-order linear non-autonomous differential equation. Multiplying both sides of (43) with $\dfrac{1}{\sqrt{V_{s,\phi}}}$ leads to

$$\frac{1}{\sqrt{V_{s,\phi}}} \dot{V}_{s,\phi} + 2h_\phi \sqrt{V_{s,\phi}} \leq -\sqrt{2}\eta_\phi. \tag{44}$$

Applying the transformation

$$\tilde{V} = \sqrt{V_{s,\phi}}, \tag{45}$$

leads to a first-order differential equation of the form

$$\dot{\tilde{V}} + h_\phi \tilde{V} \leq -\frac{\eta_\phi}{\sqrt{2}}. \tag{46}$$

Keeping in mind that the initial value of $\tilde{V}(t)$ at time $t = 0$ is $\tilde{V}(0)$, the solution of this non-homogeneous linear differential equation results in

$$\tilde{V}(t) \leq \left(\tilde{V}(0) + \frac{\eta_\phi}{\sqrt{2}h_\phi} \right) \exp^{-h_\phi t} - \frac{\eta_\phi}{\sqrt{2}h_\phi}. \tag{47}$$

Transforming back this solution in terms of the original Lyapunov function $V_{s,\phi}(t)$ leads to

$$V_{s,\phi}(t) \leq \left[\left(\sqrt{V_{s,\phi}(0)} + \frac{\eta_\phi}{\sqrt{2}h_\phi} \right) \exp^{-h_\phi t} - \frac{\eta_\phi}{\sqrt{2}h_\phi} \right]^2. \tag{48}$$

Consequently, $V_{s,\phi}(t)$ reaches zero in a finite time t_r bounded by

$$t_r \leq \frac{1}{h_\phi} \ln\left[\frac{\sqrt{2}h_\phi}{\eta_\phi}\left(\sqrt{V_{s,\phi}(0)} + \frac{\eta_\phi}{\sqrt{2}h_\phi}\right)\right]. \tag{49}$$

Here, it becomes obvious that the reaching time is proportional to the natural logarithmic of the square root of the initial value, i.e.$\sqrt{V_{s,\phi}(0)}$. This is in contrast to the case where only the switching term is employed and reaching time is proportional to the square root of the initial value $\sqrt{V_{s,\phi}(0)}$ only [12, 20, 22]. Therefore, condition (43) guarantees a fast finite reaching time. The same procedure can be repeated for the sliding manifold for the pitch axis and a finite reaching time can be guaranteed. It is worth mentioning that the reaching time condition is generally applicable for all sliding mode control design techniques where the finite-time convergence is achieved using a combination of a damping term with a switching term as already introduced in (42).

After reaching the sliding surface $s_i = 0$, $i \in \{\phi, \psi\}$, in finite time $t < t_r$, the closed-loop error dynamics of the azimuth axis and the pitch axes are governed by the following set of state equations

$$\begin{bmatrix} \dot{e}_i \\ \dot{r}_i \end{bmatrix} = \begin{bmatrix} -k_i & 1 \\ -1 + k_i c_i & -c_i \end{bmatrix} \begin{bmatrix} e_i \\ r_i \end{bmatrix}. \tag{50}$$

The characteristic polynomial of the error dynamics results in

$$p_{BS\text{-}SMC}(s) = s^2 + (k_i + c_i)s + 1, \tag{51}$$

which satisfies Hurwitz's stability criterion for strictly positive control gains $k_i > 0$ and $c_i > 0$. The eigenvalues of the closed-loop error dynamics during an ideal sliding mode are, hence, located in the left half s-plane, thus the asymptotic stability of the overall closed-loop system is guaranteed.

The sliding mode control suffers from the chattering phenomenon caused by fast switching actions introduced by the $\mathrm{sgn}(s)$ function and may lead to the excitation of unmodelled high-frequency dynamics. To counteract this effect, smooth switching functions $\tanh(s_i/\epsilon)$ with a strictly positive constant ϵ—representing a boundary layer thickness—are utilised. The chattering reduction depends on the value of ϵ at the cost of robustness. By using a large value for the boundary layer thickness ϵ the reaching time increases. This is due to the fact that the control input within the boundary thickness changes in a smooth way rather in a fast switching way. Therefore, the boundary layer thickness should be carefully selected. A typical value of $\epsilon \ll 1$ is chosen for the boundary layer thickness.

3.2 Adaptive Backstepping Control Design

To compensate the unknown lumped disturbance torques z_ϕ and z_ψ, appropriate adaptive control laws are designed for their estimation. On choosing single integrators as disturbance models, which proved advantageous in many applications, the corresponding dynamics are governed by the following relationship

$$\dot{z}_\phi = 0 \quad \text{and} \quad \dot{z}_\psi = 0.$$

Note that the integrators are driven by the output errors in observer or filter schemes. Using the recursive nature of the backstepping control, the design procedure for the adaptive backstepping control for TRAS is performed in two steps.

Step 1:
For brevity, any derivations in this step are omitted because this step is similar to the first step of the backstepping-based sliding mode control design scheme presented in Sect. 3.1.

Step 2:
To stabilise r_ϕ and r_ψ dynamics as well as to carry out the design of the adaptive laws for the lumped disturbances, the Lyapunov candidate V_2 and the corresponding differentiation $\dot{V}_2$ w.r.t. time are considered

$$V_2 = \frac{1}{2}e_\phi^2 + \frac{1}{2}r_\phi^2 + \frac{1}{2}\tilde{z}_\phi \Gamma_\phi^{-1}\tilde{z}_\phi + \frac{1}{2}e_\psi^2 + \frac{1}{2}r_\psi^2 + \frac{1}{2}\tilde{z}_\psi \Gamma_\psi^{-1}\tilde{z}_\psi, \tag{52}$$

$$\dot{V}_2 = \underbrace{e_\phi \dot{e}_\phi + r_\phi \dot{r}_\phi + \tilde{z}_\phi \Gamma_\phi^{-1}\dot{\tilde{z}}_\phi}_{\dot{V}_\phi} + \underbrace{e_\psi \dot{e}_\psi + r_\psi \dot{r}_\psi + \tilde{z}_\psi \Gamma_\psi^{-1}\dot{\tilde{z}}_\psi}_{\dot{V}_\psi}. \tag{53}$$

The strictly positive parameters Γ_ϕ and Γ_ψ represent the adaptation gains and determine the convergence speed of the estimated values to their true ones. In order to derive the control law in a simpler way, expression (53) is split into two terms denoted by $\dot{V}_\phi$ and $\dot{V}_\psi$. The estimation errors and the corresponding time derivatives of the disturbance torques are given by

$$\begin{aligned} \tilde{z}_\phi &= z_\phi - \hat{z}_\phi, & \dot{\tilde{z}}_\phi &= \dot{z}_\phi - \dot{\hat{z}}_\phi = -\dot{\hat{z}}_\phi, \\ \tilde{z}_\psi &= z_\psi - \hat{z}_\psi, & \dot{\tilde{z}}_\psi &= \dot{z}_\psi - \dot{\hat{z}}_\psi = -\dot{\hat{z}}_\psi. \end{aligned} \tag{54}$$

Regarding the lumped disturbance torque of the azimuth axis, a thorough analysis will be presented in the sequel for the derivation of the control law and the adaptive law. Considering

$$\dot{V}_\phi = e_\phi \dot{e}_\phi + r_\phi \dot{r}_\phi + \tilde{z}_\phi \Gamma_\phi^{-1}\dot{\tilde{z}}_\phi, \tag{55}$$

substituting (13), (24) and (54) into (55) leads to

$$\begin{aligned}\dot{V}_\phi &= e_\phi(-k_\phi e_\phi + r_\phi) + r_\phi\left(f_2(\mathbf{x}) + \frac{l_t\cos(\psi)}{J_\phi}F_\phi + \frac{1}{J_\phi}z_\phi - k_\phi^2 e_\phi + k_\phi r_\phi - \ddot{\phi}_d\right) \\ &\quad - \tilde{z}_\phi \Gamma_\phi^{-1}\dot{\hat{z}}_\phi, \\ &= -k_\phi e_\phi^2 + r_\phi\left(e_\phi + f_2(\mathbf{x}) + \frac{l_t\cos(\psi)}{J_\phi}F_\phi - k_\phi^2 e_\phi + k_\phi r_\phi - \ddot{\phi}_d\right) \\ &\quad + z_\phi\left(\frac{1}{J_\phi}r_\phi - \Gamma_\phi^{-1}\dot{\hat{z}}_\phi\right) + \hat{z}_\phi\Gamma_\phi^{-1}\dot{\hat{z}}_\phi. \end{aligned} \tag{56}$$

Now, the update law for the estimation of the disturbance torque z_ϕ can be stated as

$$\dot{\hat{z}}_\phi = \frac{1}{J_\phi}\Gamma_\phi r_\phi. \tag{57}$$

Substituting back the parameter update law into (56) leads to

$$\dot{V}_\phi = -k_\phi e_\phi^2 + r_\phi \underbrace{\left(e_\phi + f_2(\mathbf{x}) + \frac{l_t\cos(\psi)}{J_\phi}F_\phi - k_\phi^2 e_\phi + k_\phi r_\phi - \ddot{\phi}_d + \frac{1}{J_\phi}\hat{z}_\phi\right)}_{-\tilde{k}_\phi r_\phi} < 0. \tag{58}$$

For asymptotic stability, the Lyapunov function must be negative definite. This condition is ensured by replacing the term within the bracket with $-\tilde{k}_\phi r_\phi$ with the strictly positive control parameter $\tilde{k}_\phi > 0$. Therefore, the control law F_ϕ is given by

$$F_\phi = \left(-(\tilde{k}_\phi + k_\phi)r_\phi - (1 - k_\phi^2)e_\phi - f_2(\mathbf{x}) - \frac{1}{J_\phi}\hat{z}_\phi + \ddot{\phi}_d\right)\frac{J_\phi}{l_t\cos(\psi)}. \tag{59}$$

Similarly, based on the same guidelines provided above for the azimuth axis, the control law for the pitch motion can be derived. Thus, the corresponding disturbance torque update law, the time derivative of the Lyapunov function and the control input are summarised as follows

$$\dot{\hat{z}}_\psi = \frac{1}{J_\psi}\Gamma_\psi r_\psi. \tag{60}$$

$$\dot{V}_\psi = -k_\psi e_\psi^2 + r_\psi \underbrace{\left(e_\psi + f_4(\mathbf{x}) + \frac{l_m}{J_\psi}F_\psi - k_\psi^2 e_\psi + k_\psi r_\psi - \ddot{\psi}_d + \frac{1}{J_\psi}\hat{z}_\psi\right)}_{-\tilde{k}_\psi r_\psi} < 0, \tag{61}$$

$$F_\psi = \left(-(\tilde{k}_\psi + k_\psi)r_\psi - (1 - k_\psi^2)e_\psi - f_4(\mathbf{x}) - \frac{1}{J_\psi}\hat{z}_\psi + \ddot{\psi}_d\right)\frac{J_\psi}{l_m}. \tag{62}$$

Subsequently, the time derivative of the Lyapunov function V_2 is stated as

$$\dot{V}_2 = -k_\phi e_\phi^2 - \tilde{k}_\phi r_\phi^2 - k_\psi e_\psi^2 - \tilde{k}_\psi r_\psi^2 < 0. \tag{63}$$

With the choice of the positive control parameters, the time derivative of the control Lyapunov function is negative definite, and the asymptotic stability of the overall closed-loop system can be guaranteed.

The closed-loop error dynamics with respect to the azimuth axis and the pitch axes are governed by the following set of state equations

$$\begin{bmatrix} \dot{e}_i \\ \dot{r}_i \\ \dot{\tilde{z}}_i \end{bmatrix} = \begin{bmatrix} -k_i & 1 & 0 \\ -1 & -\tilde{k}_i & \frac{1}{J_i} \\ 0 & -\frac{1}{J_i}\Gamma_i & 0 \end{bmatrix} \begin{bmatrix} e_i \\ r_i \\ \tilde{z}_i \end{bmatrix}, \tag{64}$$

with $i \in \{\phi, \psi\}$. The characteristic polynomial for the error dynamics is given by

$$p_{ABS} = s^3 + (k_i + \tilde{k}_i)s^2 + \left(1 + k_i\tilde{k}_i + \frac{1}{J_i^2}\Gamma_i\right)s + \frac{k_i}{J_i^2}\Gamma_i. \tag{65}$$

Since the parameters $k_i, \tilde{k}_i, \Gamma_i$ as well as the moment of inertia J_i are strictly positive, the Hurwitz stability criterion is satisfied. Therefore, the eigenvalues of the closed-loop error dynamics are located in the left half s-plane and the tracking error goes asymptotically to zero. Here, the control gains $k_i, \tilde{k}_i$ and Γ_i determine the convergence rate. Using large control gains, it is possible to increase the decay rate; an asymptotic convergence characteristic, however, is always present. In contrast to this fact, the backstepping-based sliding mode control guarantees a finite-time convergence based on the reaching condition.

4 State and Disturbance Estimation

As the backstepping-based sliding mode control laws (35) and (37) require the knowledge of the immeasurable angular velocities as well as the unknown lumped disturbance torques, a discrete-time EKF is employed for the estimation tasks. In the case of the adaptive backstepping control laws (59) and (62), the angular velocities are estimated with the help of a robust sliding mode differentiator, whereas the disturbance torques are estimated using the corresponding adaptive laws. The discussion in this section focusses on the implementation of both the EKF and the robust sliding mode differentiator.

4.1 Discrete-Time Extended Kalman Filter

For the estimation of the lumped disturbance torques, the integrator disturbance models are introduced according to

$$\dot{z}_\phi = 0, \text{ and } \dot{z}_\psi = 0. \tag{66}$$

Note that these disturbance models are excited in the case of output errors between the measured and the estimated output variables. The state vector of the extended system representation results in

$$\mathbf{x}_e = \left[\phi \ \dot{\phi} \ \psi \ \dot{\psi} \ z_\phi \ z_\psi \right]^T, \tag{67}$$

and the measurement vector becomes

$$\mathbf{y}_m = \mathbf{C}_{m,e}\, \mathbf{x}_e = \begin{bmatrix} 1\,0\,0\,0\,0\,0 \\ 0\,0\,1\,0\,0\,0 \end{bmatrix} \mathbf{x}_e. \tag{68}$$

Given the continuous-time state equation of the extended system

$$\dot{\mathbf{x}}_e = \mathbf{f}(\mathbf{x}_e, \mathbf{u}), \tag{69}$$

an explicit Euler time discretization of (69) and an introduction of additive noise processes lead to the following discrete-time state-space representation used for the EKF design

$$\mathbf{x}_{e,k+1} = \underbrace{\mathbf{x}_{e,k} + T_s \mathbf{f}_k(\mathbf{x}_{e,k}, \mathbf{u}_k)}_{\boldsymbol{\varphi}_k(\mathbf{x}_{e,k}, \mathbf{u}_k)} + \mathbf{w}_k, \tag{70}$$

$$\mathbf{y}_{m,k} = \mathbf{C}_{m,e} \mathbf{x}_{e,k} + \mathbf{v}_k. \tag{71}$$

Here, T_s denotes the sampling time, $\mathbf{x}_{e,k}$ the extended state vector, $\mathbf{u}_k$ the control input vector, and $\mathbf{y}_{m,k}$ the measured output at discrete-time t_k. Furthermore, the process noise and the measurement noise are given by $\mathbf{w}_k$ and $\mathbf{v}_k$, respectively. Both are assumed to be zero-mean Gaussian white noise processes with zero cross-correlation. The vanishing cross-correlation leads to diagonal covariance matrices $\mathbf{Q}_k$ and $\mathbf{R}_k$ characterising the process noise $\mathbf{w}_k$ and the measurement noise $\mathbf{v}_k$, respectively. Figure 3 shows that the implementation of the discrete-time EKF can be divided into two stages, namely a prediction stage and an innovation stage [21]. The error covariance matrix is denoted by $\mathbf{P}_k$. The algorithm for the discrete-time EKF can be summarised at each time t_k as follows, cf. [21]:

- State prediction

$$\tilde{\mathbf{x}}_{e,k+1} = \boldsymbol{\varphi}_k(\hat{\mathbf{x}}_{e,k}, \mathbf{u}_k) \tag{72}$$

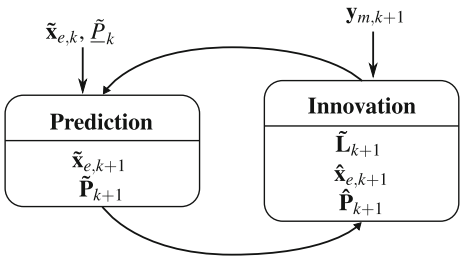

Fig. 3 Implementation of the discrete-time EKF

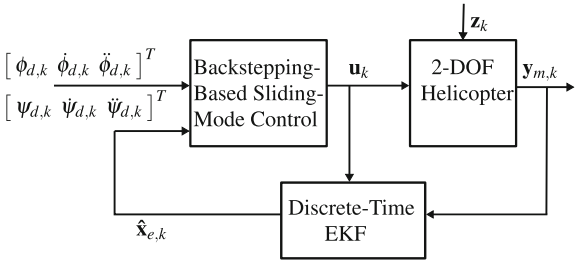

Fig. 4 Implementation scheme of the backstepping-based sliding mode control in combination with the discrete-time EKF

- Prediction of the error covariance matrix $\tilde{\mathbf{P}}_{k+1}$

$$\tilde{\mathbf{P}}_{k+1} = \boldsymbol{\Phi}_k \hat{\mathbf{P}}_k \boldsymbol{\Phi}_k^T + \mathbf{Q}_k \ , \text{ with } \ \boldsymbol{\Phi}_k = \frac{\partial \boldsymbol{\varphi}_k(\mathbf{x}_{e,k}, \mathbf{u}_k)}{\partial \mathbf{x}_{e,k}}\Big|_{\hat{\mathbf{x}}_{e,k}} \tag{73}$$

- Update of the gain matrix $\tilde{\mathbf{L}}_{k+1}$

$$\tilde{\mathbf{L}}_{k+1} = \tilde{\mathbf{P}}_{k+1} \mathbf{C}_{m,e}^T \left(\mathbf{C}_{m,e} \tilde{\mathbf{P}}_{k+1} \mathbf{C}_{m,e}^T + \mathbf{R}_k \right)^{-1} \tag{74}$$

- Update of the state vector $\hat{\mathbf{x}}_{e,k+1}$

$$\hat{\mathbf{x}}_{e,k+1} = \tilde{\mathbf{x}}_{e,k+1} + \tilde{\mathbf{L}}_{k+1} \left(\mathbf{y}_{m,k+1} - \mathbf{C}_{m,e} \tilde{\mathbf{x}}_{e,k+1} \right) \tag{75}$$

- Update of the error covariance matrix for the next sampling interval

$$\hat{\mathbf{P}}_{k+1} = \left(\mathbf{I} - \tilde{\mathbf{L}}_{k+1} \mathbf{C}_{m,e} \right) \tilde{\mathbf{P}}_{k+1} \tag{76}$$

The block diagram of the backstepping-based sliding control along with the EKF in depicted in Fig. 4.

4.2 Robust Sliding Mode Differentiator

The real differentiation using a DT1-system is sensitive to input noise. On the one hand, choosing a low cut-off frequency reduces the negative impact of high-frequency noise. On the other hand, it introduces a significant and undesired time delay. Accordingly, a high cut-off frequency results in small time delay at the cost of high-frequency noise in the output signal. This trade-off between noise and time delay in the estimation of the angular velocities could even lead to instability [13]. For the estimation of the angular velocities as required for implementation of the adaptive backstepping control, Levant's differentiator—based on a robust exact differentiation via sliding mode techniques—is employed [6, 13, 14]. The exact derivatives are calculated by successive implementation of a robust exact first-order differentiator based on a second-order sliding mode control. The finite-time convergence of this robust differentiator is proved in [13]. Provided that γ is the maximum magnitude of the measurement noise, the accuracy of the differentiator is proportional to $\gamma^{1/2}$ for the second time-derivative of the applied signal. The design procedure for the estimation of the exact differentiation of the angular velocity $\dot{\phi}$ is outlined in the following. Consider the azimuth angle ϕ as a basis signal with the third time-derivative having a known Lipschitz constant L. The robust sliding mode differentiator aiming at the estimation of $\dot{\phi}(t)$, $\ddot{\phi}(t)$ and $\dddot{\phi}(t)$ is such a way that it is exact in the absence of measurement noise. A second-order differentiator for the input ϕ with $|\dddot{\phi}(t_0)| \leq L$ according to [14] is given by

$$\begin{aligned} \dot{z}_0 &= \nu_0, \quad \nu_0 = -3L^{1/3}|z_0 - \phi|^{2/3}\,\mathrm{sgn}(z_0 - \phi) + z_1, \\ \dot{z}_1 &= \nu_1, \quad \nu_1 = -1.5L^{1/2}|z_1 - \nu_0|^{1/2}\,\mathrm{sgn}(z_1 - \nu_0) + z_2, \\ \dot{z}_2 &= -1.1L\,\mathrm{sgn}(z_2 - \nu_1), \end{aligned} \tag{77}$$

with $[z_0\ z_1\ z_2]^T = [\hat{\phi}\ \dot{\hat{\phi}}\ \ddot{\hat{\phi}}]^T$. Similarly, the angular velocity for the pitch angle can be easily estimated using the robust sliding mode differentiation.

Figure 5 shows the implementation scheme of the controller in combination with the robust sliding mode differentiator.

The closed-loop stability of the overall control structure consisting of the nonlinear control techniques along with the estimators has been investigated thoroughly in simulations.

5 Simulation and Experimental Results

In this section, the proposed backstepping-based sliding mode control (BS-SMC) and the adaptive backstepping (ABS) control laws in combination with the EKF and the robust state differentiators, respectively, are investigated by both simulations and experimental evaluations. To guarantee realistic simulation results, the system model is extended with measurement noise concerning the incremental encoders for